Front. Phys. China, 2010, 5(3): 260–265
DOI 10.1007/s11467-010-0016-8

MINI-REVIEW ARTICLE

Photonic crystal surface mode microcavities

Jing WANG (王静), **Min YAN** (严敏), **Min QIU** (仇旻)†

Laboratory of Optics, Photonics and Quantum Electronics, Department of Microelectronics and Applied Physics, Royal Institute of Technology (KTH), Electrum 229, 16440 Kista, Sweden
E-mail: min@kth.se

Received February 9, 2010; accepted March 10, 2010

Our recent research on surface mode optical microcavities based on two-dimensional photonic crystals (PhCs) was reviewed in this paper. We presented the design, fabrication and characterization of high quality (Q) factor surface mode microcavities. Realizations of these PhCs were based on both amorphous silicon-on-insulator (SOI) structures and crystalline SOI structures.

Keywords photonic crystal (PhC) surface mode microcavities, three-dimensional (3-D) finite-difference time-domain (FDTD), quality-factors

PACS numbers 42.70.Qs, 42.82.Bq

Contents

1 Introduction 260
2 Design for the PhC surface mode microcavities 261
2.1 Surface mode microcavities in a square PhC slab 261
2.2 Surface mode microcavities in a triangular PhC slab 262
3 Experimental demonstration of surface mode microcavities 262
3.1 Surface mode PhC microcavities on an amorphous SOI substrate 262
3.2 Surface mode microcavities on a crystalline SOI substrate 264
4 Conclusions 265
Acknowledgements 265
References 265

1 Introduction

Photonic crystals are artificial electromagnetic materials that have periodic refractive index modulations [1, 2]. A photonic band gap can exist in a photonic crystal (PhC) for certain frequency ranges, where the light prorogations are forbidden, due to the diffraction of electromagnetic waves by the periodic structures [3–7]. This important property leads to many new physical phenomena and the potential applications in optoelectronics.

Kossel in 1969 demonstrated that surface waves can exist in the interface between a periodic structure and a homogenous material [8]. For PhC surface waves, their frequencies are within the photonic band gap of the PhC, and light propagates along the interface between air (or other dielectric materials) and the PhC [3, 9]. Confinement of the surface waves at the interface is due to the PhC's photonic band gap which prevents light from penetrating into the PhC, and also due to the fact that the dispersion of light is below the light line of the material in the other half domain.

High Q microcavities are of great interest in many applications in optical communications, bio-photonics, quantum optics, etc. Most of the high Q PhC microcavities are realized in PhC slab structures, which are two-dimensional (2-D) PhCs but truncated in the third (invariant) dimension. If such a slab has an effective index higher than that of the background material, the index guiding mechanism will provide light confinement in the third dimension. Many research works have been devoted to the designs and experimental demonstrations of high-Q factor PhC microcavities in silicon-based PhC slab structures. The standard microelectronic (silicon) fabrication technologies provide the possibility of achieving extremely high-Q factor PhC microcavities (e.g., see Refs. [7, 9]). Among many designs of microcavities, PhC surface mode cavities have attracted certain attention due to their special optical properties, in particular, as open cavities, where one of the in-plane boundaries is exposed to the exterior. Here, we present our recent research efforts, theoretically and experimentally, on the properties of surface wave microcavities.

The paper is organized as follows. In Section 2 we

show the designs of high-Q surface mode microcavities based on PhCs with a square and a triangular lattice. In Section 3 experimental results of surface mode microcavities realized on both the amorphous and the crystalline silicon-on-insulator (SOI) substrate are presented. The resonate frequencies and Q factors as a function of the cavities lengths are investigated. In Section 4 the conclusions are presented.

2 Design for the PhC surface mode microcavities

Because of the existence of photonic band gaps, surface modes can propagate in the interface between a PhC and air. If we terminate the surface edges by reflecting mirrors, a cavity is formed for the surface modes [10, 11]. Our designs for surface mode microcavities are shown in Fig. 1. For a 2-D square PhC slab, the edge rods act as reflecting mirrors in the y direction, while the edge air holes in a 2-D triangular PhC slab act as the mirrors. We denote the lengths of the cavities as L. The surface mode cavities in PhCs can be considered as the conventional Fabry–Péot cavities, i.e., the phase accumulated in the round trip $\Phi = 2kL + 2\Delta\phi$, Where k is the wave vector, $\Delta\phi$ is the phase shift due to the reflecting mirror. For the finite-size PhC surface mode cavities, only the modes satisfying the resonant conditions, i.e. $\Phi = 2\pi \cdot N$, can survive, becoming the surface resonant modes.

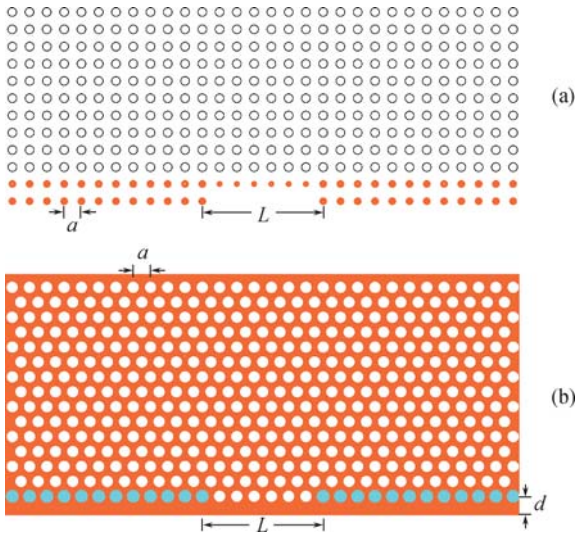

Fig. 1 Top views of the microcavities composed by **(a)** a 2-D square PhC slab and **(b)** a 2-D triangular PhC slab.

2.1 Surface mode microcavities in a square PhC slab

We employ the 3-D FDTD method with the perfectly matched layer boundaries to investigate the behaviors of surface resonant modes. First, we take the PhC slab with square lattice as an example. The radius of the dielectric rods is $R = 0.2a$, where a is the lattice constant, and the slab thickness is $2a$. The dielectric constant is set to $\varepsilon = 11.56$. The surface mode cavity is formed by slightly reducing the radius of the rods ($R_d = 0.15a$) at the boundaries. The dispersion characteristic of the surface mode is plotted on the band diagram as in Fig. 2(a). The shadow regions in the figure are the projected band structure for the TM modes. There is only one mode that has the group velocity v_g zero when wave vector $k = \pi/a$. Based on our simulations, the Q factor of the resonant mode at $k = \pi/a$ is much larger than other cavity modes [12]. In Fig. 3(a) the z component of the electric field of a high-Q resonant mode in a cavity with length $L = 11a$ is shown. The horizontal and vertical cross sections of the electric field z component at the center plane of third axis (z= 0) and at the plane center of the surface defects are depicted. The high mode has an angular frequency of $0.3599(a/\lambda)$ and a quality factor $Q = 1.24 \times 10^4$. As shown in Fig. 3(a), the z components of the electric field in horizontal and vertical cross section of the surface defect are almost completely confined in the center of the cavity.

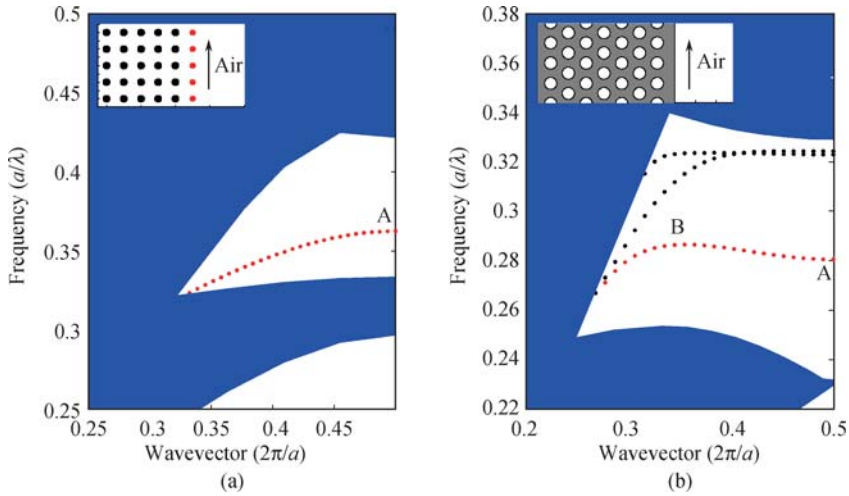

Fig. 2 The surface mode band structures for **(a)** a square PhCs slab with dielectric rods in air, and **(b)** a 2-D triangular PhC of air holes. Reprinted with permission from Ref. [10]. Copyright © 2003 American Institute of Physics.

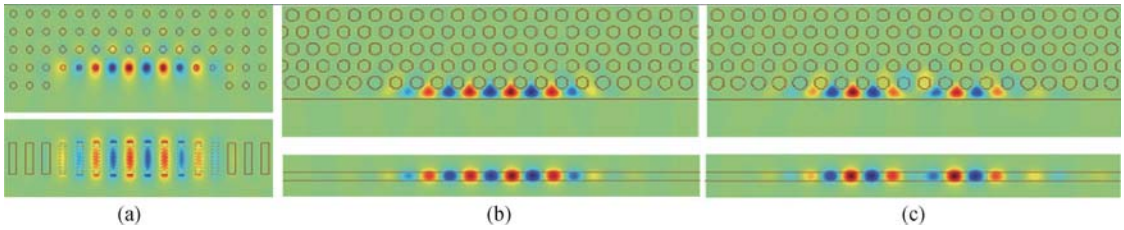

Fig. 3 **(a)** E_z field cross sections of the surface resonant mode in the square PhC slab. **(b)** and **(c)** H_z field cross sections of two resonant modes corresponding to $\omega_b = 0.2816(a/\lambda)$ and $\omega_c = 0.2841(a/\lambda)$ in the triangular PhC slab. Solid lines are outlines of the rods/holes/slabs. Reprinted with permission from Ref. [10]. Copyright © 2003 American Institute of Physics.

The calculated Q factor corresponding to the wave vector $k = \pi/a$ as a function of cavity lengths (L) is present in Fig. 4(a). For the square-lattice PhC microcavity case, with the increase of the cavity lengths, the Q factor becomes larger. While the cavity length increases from $4a$ to $12a$, the Q factor increases significantly, from the order of 10^2 to the order of 10^4. Furthermore, as our simulations reveal, with the increase of the cavity length, the resonant frequency converges to ω_0, which corresponds to the zero group velocity surface mode in the PhC slab.

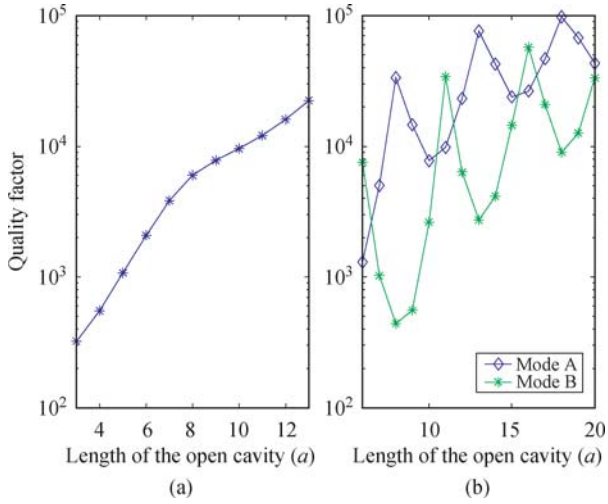

Fig. 4 Quality factors as a function of the cavities length (L) for surface mode microcavities in **(a)** a square PhC slab and **(b)** a triangular PhC slab. Reprinted with permission from Ref. [10]. Copyright © 2003 American Institute of Physics.

2.2 Surface mode microcavities in a triangular PhC slab

Figure 1 (b) shows a surface mode microcavity in a PhC slab whose air holes are in a triangular lattice. Similar structures are subsequently fabricated and characterized, as will be presented in Section 3. In order to describe the shape of the truncated slab, we introduce the truncated parameter d, which is the distance between the first line hole center to the boundary of the slab, as shown in Fig. 1(b). As an example, the hole radius is set to be $0.3a$, and the slab thickness being $0.6a$. The dielectric constant is $\varepsilon = 11.56$ and the truncated parameter is set to $d = \sqrt{3}a/2$. Based on our simulations, the Q factor is quite sensitive to the truncated parameter d. Figure 2(b) shows the dispersion relations of the transverse electric (TE) surface modes. There are three surface modes in the band gap. For simplicity, we only discuss the surface mode in the frequency range between $0.26(a/\lambda)$ and $0.30(a/\lambda)$. From our 3-D FDTD simulation results, there are two high Q surface modes, corresponding to the zero group velocity modes for the cavity length of $L = 11a$, i.e., mode A and mode B. Mode A has the resonant frequency of $\omega_a = 0.2816(a/\lambda)$ with a wave vector $k_a = \pi/a$, while mode B has $\omega_b = 0.2841(a/\lambda)$ with a wave vector $k_b = 0.71\pi/a$. We present the cross sections of the magnetic fields z component for mode A and mode B in Fig. 3(b) and (c), respectively. The upper and bottom figures are magnetic fields at the horizontal and vertical cross sections at the plane of $z = 0$ and at the vertical y–z plane.

The Q factors and the resonant frequencies are plotted as a function of the cavity length L for both modes in Fig. 4 (b). As L increases, the Q factors for both two modes fluctuate. The reason is due to the complicated reflective interfaces, and for the Fabry–Perot condition $\Phi = 2kL + 2\Delta\phi$, the phase shift $\Delta\phi$ is no longer close to π for both modes. This is different from the situation for the square PhC surface mode microcavities. From the simulation results, the highest Q factor for mode A is 9.78×10^4 when $L = 18a$, while the highest Q factor is 5.73×10^4 for mode B when $L = 16a$.

3 Experimental demonstration of surface mode microcavities

In this section, we present the fabrication and the characterization of surface mode microcavities in triangular-lattice PhC slab structures, realized on both amorphous and crystalline SOI substrates.

3.1 Surface mode PhC microcavities on an amorphous SOI substrate

The schematic of the experimentally demonstrated PhC surface mode microcavity is shown in Fig. 5. The microcavity is side coupled to a silicon wire waveguide, which have a wide end initially and is taped down to a single-mode dimension close to the cavity. For the amorphous SOI substrate, the silica buffer layer has the thickness of

6 μm, which can efficiently prevent the light from leaking to the bottom silicon layer. The silicon layer on top has a thickness of 280 nm. PhC microcavities are patterned on the silicon layer.

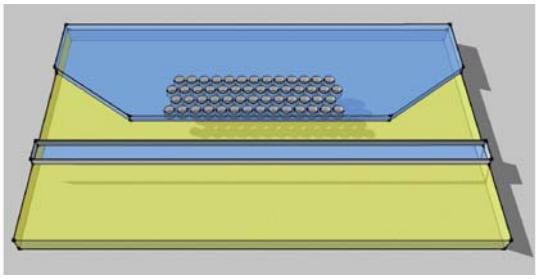

Fig. 5 Schematic of a PhC surface mode cavity side coupled to a silicon waveguide in the SOI structure.

The devices are fabricated as the following three steps [13]. First, the low temperature (300°C) plasma enhanced chemical vapor deposition (PECVD) is utilized to deposit a 6 μm silica buffer layer on a silicon wafer. A 280-nm-thick hydrogenated amorphous silicon (α-Si:H) is then deposited on its top. The measured root-mean-square surface roughness of the amorphous silicon is below 2 nm. A ZEP520A resist is then coated on the amorphous SOI substrate and PhC surface mode cavities are patterned with electron-beam (e-beam) lithography. We do a series of dose tests to reduce the design and target size differences and proximity effect. After the dose test, the lattice constant a of PhC is 380 nm and the regular air holes diameter of PhC is 228 nm. The Fabry–Pérot cavity length is estimated as $L \approx 26a = 9.88$ μm. The reflecting mirrors along the PhC edge are introduced by slightly enlarging the radii of six surface holes at both ends. The air gap between the PhC and the waveguide is 200 nm, and the truncated parameter d is controlled as 180 nm. The silicon wire is initially 2 μm and gradually tapered down to single-mode dimension of 425 nm when coupled to the PhC microcavities. After coupling to the microcavities, the silicon wire is tapered back to 2 μm. In the last step, the patterns on the resist are transferred to the top amorphous silicon layer in an inductively coupled plasma reactor. The SEM photo of a fabricated PhC surface mode microcavity is shown in Fig. 6.

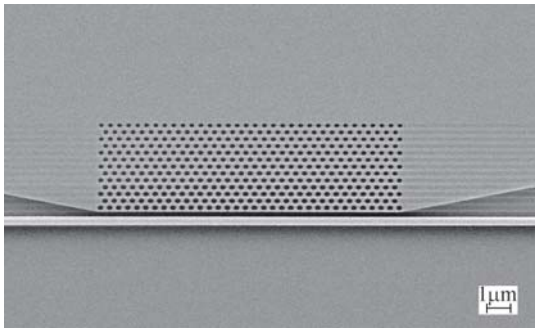

Fig. 6 SEM photo of a surface mode microcavity on an amorphous SOI structure.

After cleaving, the fabricated samples are characterized by the end-fire coupling setup. The light source is amplified spontaneous emission source with the infrared signal between 1.52 μm and 1.61 μm. The light is coupled into the waveguide from a polarization maintaining fiber through the graded-index lens. The output signal is collected by a multimode fiber, which is connected to an optical spectrum analyzer. In this measurement method, a Glan–Thompson polarizing prism is placed in front of the sample so that only the TE mode of the signal is incident to the waveguide. The resolution of the spectrum analyzer is set to 0.2 nm and the average time of the measurement is 10 to obtain the stable signal.

The measured spectrum of the PhC surface mode microcavity is shown in Fig. 7. The transmission spectrum is normalized with respect to the transmission spectrum of the same waveguide but without a side-coupled PhC microcavity. The transmission dip in the spectrum is around 1580 nm. From the full width at half maximum $\Delta\lambda$ and the central drop wavelength λ_0, we obtain the total Q factor of the microcavity by $Q_{\rm tot} = \lambda_0/\Delta\lambda \approx 600$. The extinction ratio E_r is more than 10 dB. From the couple mode theory [14], E_r is given by the equation

$$E_r = -10\log_{10}\frac{P_{\rm out}(\lambda_0)}{P_{\rm in}(\lambda_0)} = -10\log_{10}\left|\frac{Q_c}{Q_i+Q_c}\right|^2 \quad (1)$$

where Q_i is the intrinsic quality factor of the cavity and Q_c is the coupling quality factor between the cavity and the waveguide. The total quality factor of the device is related to Q_i and Q_c by

$$\frac{1}{Q_{\rm tot}} = \frac{1}{Q_i} + \frac{1}{Q_c} \quad (2)$$

From Eqs. (1) and (2), the intrinsic quality factor is estimated to be $Q_i \approx 2000$.

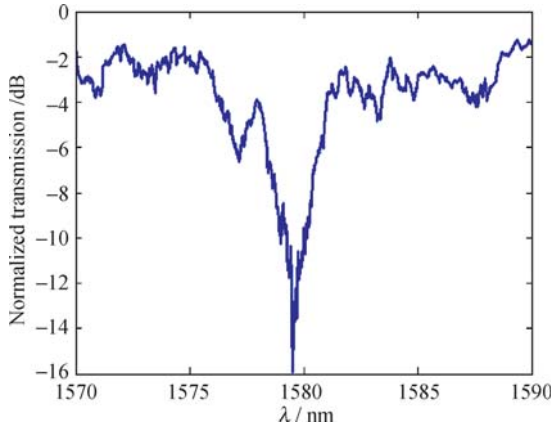

Fig. 7 Normalized transmission spectrum for the surface mode microcavity fabricated on an amorphous SOI substrate. Reprinted with permission from Ref. [13]. Copyright © 2007 American Institute of Physics.

The quality factors of PhC surface mode microcavity are thus very low on an amorphous SOI substrate. There are three main reasons behind the low Q factors. One

is the inherent high loss possessed by amorphous silicon. Fabrication imperfection also contributes to the loss of the device. The other major reason is the multiple modes present in the drop frequencies region, as one can see in the measurement spectrum.

3.2 Surface mode microcavities on a crystalline SOI substrate

In order to improve the Q factors, we also fabricated PhC surface mode microcavities on crystalline SOI structures. The PhC microcavities and waveguides are fabricated on a crystalline SOI wafer with a top crystalline silicon layer of thickness 250 nm and a buried oxide layer of thickness 3 μm. Samples with microcavity lengths of $L = 24a$ and $L = 28a$ are fabricated by standard electron-beam lithography similar to the surface mode cavity in Section 3.1. The truncated parameter d for both PhCs is 380 nm. The lattice constant a of the PhC slab is 380 nm for $L = 24a$, and a=390 nm for $L = 28a$, respectively. The regular air hole radius r=120 nm for $L = 24a$, and r=122 nm for $L = 28a$, respectively. The reflecting mirrors along the PhC edge are again introduced by slightly enlarging the radii of six first line holes at both ends, the radius of 125 nm for $L = 24a$ and 128 nm for $L = 28a$, respectively.

To characterize the PhCs microcavities, we measure the transmission through the waveguides by the vertical fiber-grating coupling method [15]. Light from a tunable laser with a wavelength range from 1530 nm to 1580 nm is first coupled to a polarizer so that only the TE mode is collected. Through the polarizer, the light is coupled into the wide waveguide via a gold grating coupler. The waveguide is initially 10 μm and taped down to 420 nm to ensure the single mode propagation when in coupling with the cavity. At the output side, another taper guides the light back to 10 μm and a fiber connected to the optical spectrum analyzer collects the light from the waveguide through another gold grating coupler. The transmission spectrum is then normalized with respect to the transmission spectrum of the same waveguide but without a side-coupled PhC microcavity.

Figure 8 shows the normalized transmission spectra for these two devices. The coupled-mode theory is applied to such two port systems to fit the curves. The transmission spectrum is in general of the Lorentzian shape and the transmission is given by the equation

$$|T|^2 = \frac{(\omega - \omega_0)^2 + \left(\frac{\omega_0}{2Q_i}\right)^2}{(\omega - \omega_0)^2 + \left(\frac{\omega_0}{2Q_{\text{tot}}}\right)^2} \tag{3}$$

where T is the transmission function; ω and ω_0 are the incident light frequency and resonant frequency, respectively. Q_i and Q_{tot} fulfill the relations as specified by

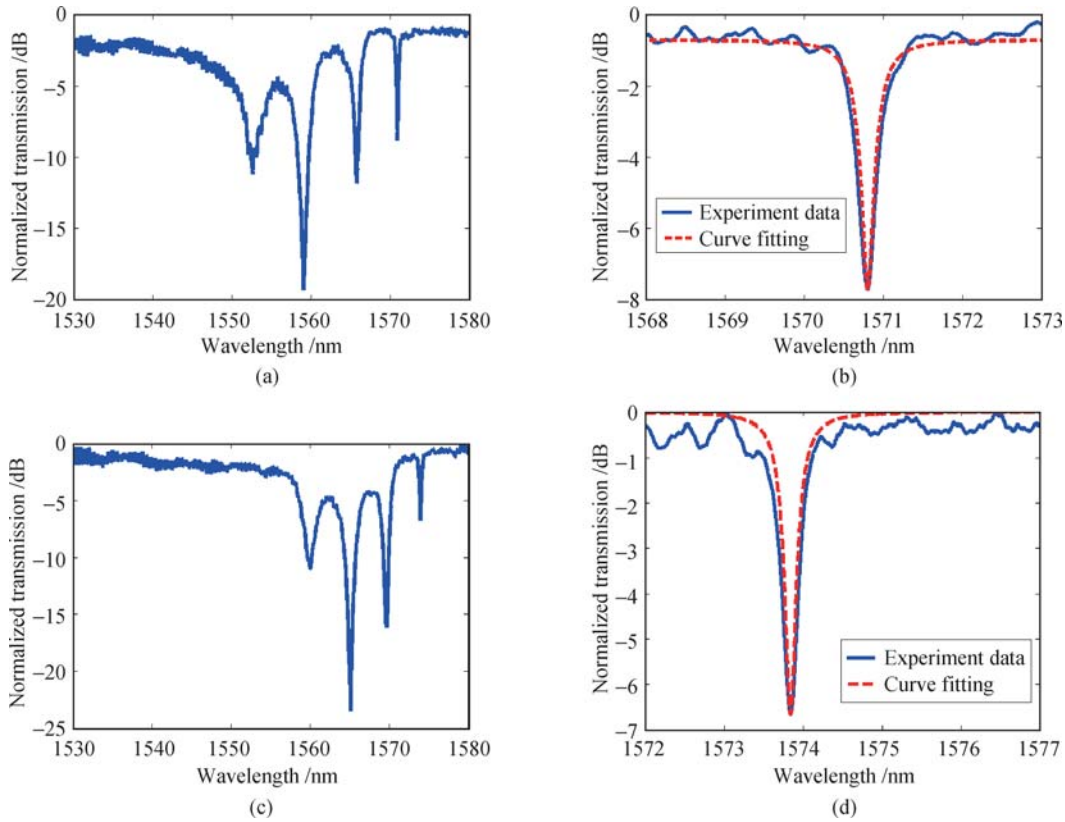

Fig. 8 Normalized transmission spectra of **(a)** broad transmission spectrum corresponding to the cavity length of 24a, **(b)** transmission spectrum and fitting curve for one of the peaks in (a), **(c)** broad transmission spectrum with the cavity length of 28a and **(d)** transmission spectrum and fitting curve for one of the peaks in (c).

Eqs. (1) and (2). Through curve fitting, for the cavity length of $24a$, the maximal value of the system Q is about 5000 and the intrinsic Q is 11 600 at 1570.8 nm. The cavity with the length of $28a$ shows the maximal system Q of 6200 and intrinsic Q of 13 400 at 1537.8 nm.

4 Conclusions

In this paper, we have systematically studied the optical microcavities based on the surface modes in 2-D PhC slabs. According to our simulations, high Q surface mode microcavities can be obtained for silicon based with either a square or a triangular lattice. We have also experimentally fabricated the designed microcavities based on PhC slabs with a triangular air hole arrangement, using both amorphous and crystalline SOI substrates. The results show that the highest intrinsic Q factor obtained is 13 400 on a crystalline SOI structure.

Acknowledgements The authors would like to thank Shan-shui Xiao and Zi-yang Zhang for the valuable discussions. This work was supported by the Swedish Foundation for Strategic Research (SSF) and the Swedish Research Council (VR).

References

1. E. Yablnovitch, Phys. Rev. Lett., 1987, 58: 2059
2. S. John, Phys. Rev. Lett., 1987, 58: 2486
3. J. D. Joannopoulos, R. D. Meade, and J. Winn, 1st Ed., Princeton: Princeton University Press, 1995
4. D. K. Armani, T. J. Kippenberg, S. M. Spillane, and K. J. Vahala, Nature, 2003, 421: 925
5. Z. Y. Zhang and M. Qiu, Opt. Express, 2004, 12: 3988
6. T. Uesugi, B. Song, T. Asano, and S. Noda, Opt. Express, 2006, 14: 377
7. B. S. Song, S. Noda, T. Asano, and Y. Akahane, Nature Materials, 2005, 4: 207
8. D. Kossel, J. Opt. Soc. Am., 1969, 56: 1434
9. J. Yang, S. H. Kim, G. H. Kim, H. G. Park, Y. H. Lee, and S. B. Kim, Appl. Phys. Lett., 2004, 84: 3016
10. S. Xiao and M. Qiu, Appl. Phys. Lett., 2003, 87: 111102
11. S. S. Xiao and M. Qiu, J. Opt. Soc. Am. B, 2007, 24(5): 1225
12. M. Ibanescu, S. G. Johnson, D. Roundy, U. Fink, and J. D. Joannopoulos, Opt. Lett., 2005, 30: 552
13. Z. Zhang, M. Dainese, L. Wosinski, M. Swillo, U. Andersson, S. Xiao, and M. Qiu, Appl. Phys. Lett., 2007, 90: 041108
14. C. Manolatou, M. J. Khan, S. Fan, P. Villeneuve, H. A. Hans, and J. D. Joannopoulos, IEEE J. Quantum Electron., 1999, 35: 1322
15. S. Scheerlinck, J. Schrauwen, F. V. Laere, D. Taillaert, D. V. Thourhout, and R. Baets, Opt. Express, 2007, 15: 9625